Remote Sensing of Environment 216 (2018) 572–585

Contents lists available at ScienceDirect

Remote Sensing of Environment

journal homepage: www.elsevier.com/locate/rse

Estimating the age and population structure of encroaching shrubs in arid/semiarid grasslands using high spatial resolution remote sensing imagery

Xin Cao, Yu Liu*, Qixin Liu, Xihong Cui, Xuehong Chen, Jin Chen

State Key Laboratory of Earth Surface Processes and Resource Ecology, Faculty of Geographical Science, Beijing Normal University, Beijing 100875, China

ARTICLE INFO

Keywords:
Shrub encroachment
Shrub age estimation model
Population structure
High spatial resolution remote sensing

ABSTRACT

Many arid and semiarid grasslands around the world are suffering from shrub encroachment to a great extent. However, the process of shrub encroachment is still poorly understood. Particularly, there has been limited historical datasets and inadequate field samples about the encroachment species. Shrub age can serve as an important indicator of the shrub encroachment history; and the population structure based on the shrub age distribution can reflect the population dynamics of an encroachment species. Using a high spatial resolution (HSR) remote sensing data, this paper estimates the age and population structure of a typical shrub, the *Caragana* genus (hereafter shrubs) in the temperate arid and semiarid grasslands of Inner Mongolia, China. The primary methods include: (1) building a shrub age estimation model considering different shrub crown growth rates affected by different precipitation regimes in the Inner Mongolian grassland; (2) identifying shrub individuals from multiple HSR remote sensing images and estimating the age of shrub individuals using the developed shrub age estimation model; (3) establishing a shrub age histogram, fitting the population structure, and calculating the survival rate and regeneration count using a negative exponential function. The results indicate that this shrub age estimation model performs better than a simple statistical regression using only the shrub crown area. Further, employing the negative exponential function for research on shrub encroachment provides supporting evidence of its effective role in capturing the population structure. Result also identifies that the survival rate increases with precipitation.

1. Introduction

Grassland is an important terrestrial vegetation type and a region with vulnerable natural environments (Scurlock and Hall, 1998). Under the influence of global climate change and human activities, over 50% of grassland ecosystems have been severely degraded (Gang et al., 2014). Grassland degradation may lead to a decrease in biodiversity (Belsky, 1992; Sala, 2000), water and soil erosion (D'Odorico et al., 2012; Li et al., 2008; Schlesinger et al., 1999), decreased net primary productivity (Huenneke et al., 2002; Zarovali et al., 2007), shrub invasion or encroachment (He et al., 2010; Mishra et al., 2015; Peng et al., 2013), and global climate change (D'Odorico et al., 2010; Kéfi et al., 2007). Shrub encroachment caused by changes in the terrestrial vegetation in arid and semiarid grasslands threatens the sustainability of grassland resources and livestock production (Eldridge et al., 2011).

Shrub encroachment is a phenomenon prevalent in arid and semiarid regions, including Africa, North America, South America, Australia, and the polar regions (Cabral et al., 2003; D'Odorico et al., 2010; Levick and Rogers, 2011; Naito and Cairns, 2011; Robinson et al., 2008; Tape et al., 2012; Van Auken, 2009). The temperate arid and semiarid grasslands of Inner Mongolia, China is such a typical area that has attracted much attention in recent decades (Peng et al., 2013; Xiong et al., 2003). From 1983 to 2011, the shrub-encroached grassland area has increased by 124% in the Xilin River Basin, while the natural grassland decreased from 8520 km^2 to 7893.12 km^2 (Han et al., 2014). One of the major encroaching shrub genera in the Inner Mongolia grasslands is *Caragana*. Shrubs of this genus are primarily distributed in continental temperate regions in Asia and the Tibetan Plateau, and about twenty *Caragana* species pervade nearly the entire area (Niu, 1999). These species include *C. microphylla* Lam., *C. korshinskii* Kom., *C. stenophylla* Pojark., and *C. intermedia* Kuang et H. C. Fu. Caragana plants are helpful for afforestation and the stabilization of sand due to their relatively high drought tolerance (Bao et al., 2015b). These plants also tend to be competitive when drought occurs, and their encroachment may lead to grassland degradation and desertification (Han et al., 2014). Scholars have noted that overgrazing is one of the primary causes of the *Caragana* encroachment (Xiong et al., 2003; Zhao et al., 2014). An effective method to study the shrub encroachment process is

* Corresponding author.
E-mail address: liuyu0213@mail.bnu.edu.cn (Y. Liu).

https://doi.org/10.1016/j.rse.2018.07.025
Received 6 November 2017; Received in revised form 17 July 2018; Accepted 21 July 2018
Available online 25 July 2018
0034-4257/ © 2018 Elsevier Inc. All rights reserved.

via long-term and dynamic monitoring. Methods for long-term monitoring include field observations in a limited area (Cipriotti and Aguiar, 2012) and interpreting multi-temporal high spatial resolution (HSR) remote sensing images (Laliberte et al., 2004). However, the lack of effective field observations and long-term HSR images severely limits such research. Therefore, understanding shrub encroachment and its spatial heterogeneity requires additional information.

Shrub encroachment in arid and semiarid grasslands increases the biomass, density, and coverage of shrubs or woody plants (Van Auken, 2009). Several studies have described the shrub encroachment as an increase in shrub cover or shrub patch growth using long-term field observations or remote sensing images (Cabral et al., 2003; Laliberte et al., 2004). Myers-Smith et al. (2011) used the maximum patch age (initiation date) to reveal the willow encroachment history. The population structure derived from the age distribution can reflect the species regeneration and mortality (Kuuseoks et al., 2001; Wiegand et al., 2000), which provides a unique perspective to understand the shrub encroachment. Understanding the population structure of shrubs establishes a methodological basis for understanding the past species development as well as predicting future scenarios (Wiegand et al., 2000). A negative exponential distribution model can describe a population structure well (Kuuseoks et al., 2001); however, building a precise model requires a sufficient amount of field samples. More samples are required to build population structure models over a large geographical scale. Discrepancies between the parameters (regeneration and survival rate) of different models can help us understand the spatial heterogeneity of the shrub encroachment process. However, shrub age is difficult to measure in a direct manner. Field sample measurement methods are labor-intensive, time-consuming, high-cost, and destructive to the species. Consequently, studying the population structure is commonly conducted within a limited geographical range and can rarely obtain satisfactory fitting results (Crisp and Lange, 1976; Dahlgren et al., 2016).

Traditional methods for determining shrub age include counting bud scale scars (Kuuseoks et al., 2001) or annual growth rings (Myers-Smith et al., 2015). Stem samples are sectioned and stained, and then a microscopic photographic technique is used to count growth rings (Büntgen et al., 2015; Schweingruber and Poschlod, 2005). However, the growth rings of shrubs may be obscure due to extreme environmental conditions and become difficult to count visually. Under certain conditions, the shrub age can be directly determined, such as in artificially planted areas (Tian et al., 2014) or during shrub regeneration after fires (Seligman and Henkin, 2000). To avoid the destructive nature of sampling stems, several shrub age estimation models have been proposed assuming that the shrub morphology is positively correlated to the shrub age (Brotherson et al., 1980; Crisp and Lange, 1976; Myers-Smith et al., 2011). However, these methods are based on field work, which means that samples are either limited or inapplicable to other geographical ranges. Acquiring an abundant number of shrub age samples at every site in a large region requires a non-destructive shrub age estimation method.

Remote sensing provides an effective method of monitoring the shrub encroachment at a large geographical scale. In recent years, various aerial images and satellite remote sensing data have been used to monitor shrub encroachment. Several methods for recognizing or identifying shrubs from these data have been developed. According to the spatial resolution of the remote sensing imagery used, these methods can be classified into two categories.

(1) Shrub coverage estimation from moderate- or low-resolution remote sensing images, such as Landsat Thematic Mapper (TM) and Moderate Resolution Imaging Spectroradiomete (MODIS). Spectral mixture analysis (SMA) is the most popular method of vegetation coverage estimation. However, shrub coverage is usually low (even lower than 10% according to our field observations of 50 m × 50 m plots) in arid and semiarid regions. Therefore, estimating the shrub fraction using the SMA is unreliable when a pure shrub endmember is not available. To produce a "pure" endmember from a mixed landscape, Sohn and Mccoy (1997) simulated a shrub endmember at the TM scale from a field shrub spectrum. Ma et al. (2015) developed an endmember spectrum purification procedure; this procedure is capable of extracting a pure endmember spectrum when it is not present in the target images of arid and semiarid environments. In addition, collinearity may lead to the SMA failure due to the spectral similarity between shrubs and grasses in a mixed shrub-and-herbaceous plant landscape (Chen et al., 2011). Multi-temporal remote sensing images can also help recognize shrubs according to the difference in phenology between invasive shrubs and native species (Wilfong et al., 2009). Shrub coverage was mapped using regression tree models derived from multi-temporal MODIS data (Selkowitz, 2010); however, the result was relatively unreliable due to the low spatial resolution. In addition, multi-angle and geometric-optical models fail to precisely estimate shrub coverage, because the contributions of shrubs and non-shrubs to the aggregate bidirectional reflectance distribution function are difficult to differentiate (Chopping et al., 2008).

(2) Individual shrub identification. In recent years, multiple HSR remote sensing satellites have been launched, such as the Worldview 2-3, QuickBird, and GeoEye-1. These HSR remote sensing images and aerial photos allow the direct identification of shrubs and the subsequent analysis of the shrub encroachment. Robinson et al. (2008) used aerial images captured from 1943 to 2004 to analyze the shrub encroachment in western Australian arid grasslands using an unsupervised classification method. HSR remote sensing images contain enhanced texture and shape information; for example, they recognize that a circular or oval shrub is distinct from grass and soil (Laliberte et al., 2004). A morphology-based delineation of shrub and tree crowns method (CANAPI) was proposed and validated on HSR images (Chopping, 2011; Duchesne et al., 2016). CANAPI identifies the crowns of trees or shrubs by searching for crescent-shaped groups of bright pixels corresponding to the sunlit parts of the crowns. Object-based image analyses incorporate spectral information and spatial arrangements (size, shape, texture, and association with neighboring objects) and work in a way similar to how people visually interpret information from images (Laliberte et al., 2004). Therefore, object-based image analysis methods are often used to identify shrub individuals from HSR remote sensing images (Laliberte et al., 2004; McGlynn and Okin, 2006; Waser et al., 2008). However, the lack of a historical data archive of HSR images poses a considerable obstacle to studying the shrub encroachment process. Recently, Isaacson et al. (2017) used tree size measured from an HSR image as an indicator to distinguish long-term and short-term hydrologic spatial processes affecting the acacia population. The challenge is to obtain quantitative dynamic information concerning shrub encroachment from individual HSR images.

This study aims to build a shrub age estimation model applicable to a large geographical range and quantify the population structure at each site based on the shrub age distribution. Accordingly, we establish a shrub age estimation model that is adapted to different geographical sites in the Inner Mongolian grassland while considering varying shrub growth rates affected by differing precipitation regimes. Shrub individuals are identified from multiple HSR imagery sources, such as images on Google Earth (GE), WorldView-2 (WV2) images and aerial photos (AP) taken from unmanned aerial vehicles. The crown area of each shrub individual is retrieved and used to estimate the age based on the shrub age estimation model. Then, we build a precise shrub population structure model using a negative exponential function for each geographical location to acquire the shrub regeneration count and survival rate. This method can improve our understanding of the shrub encroachment process and its spatial heterogeneity in regions with

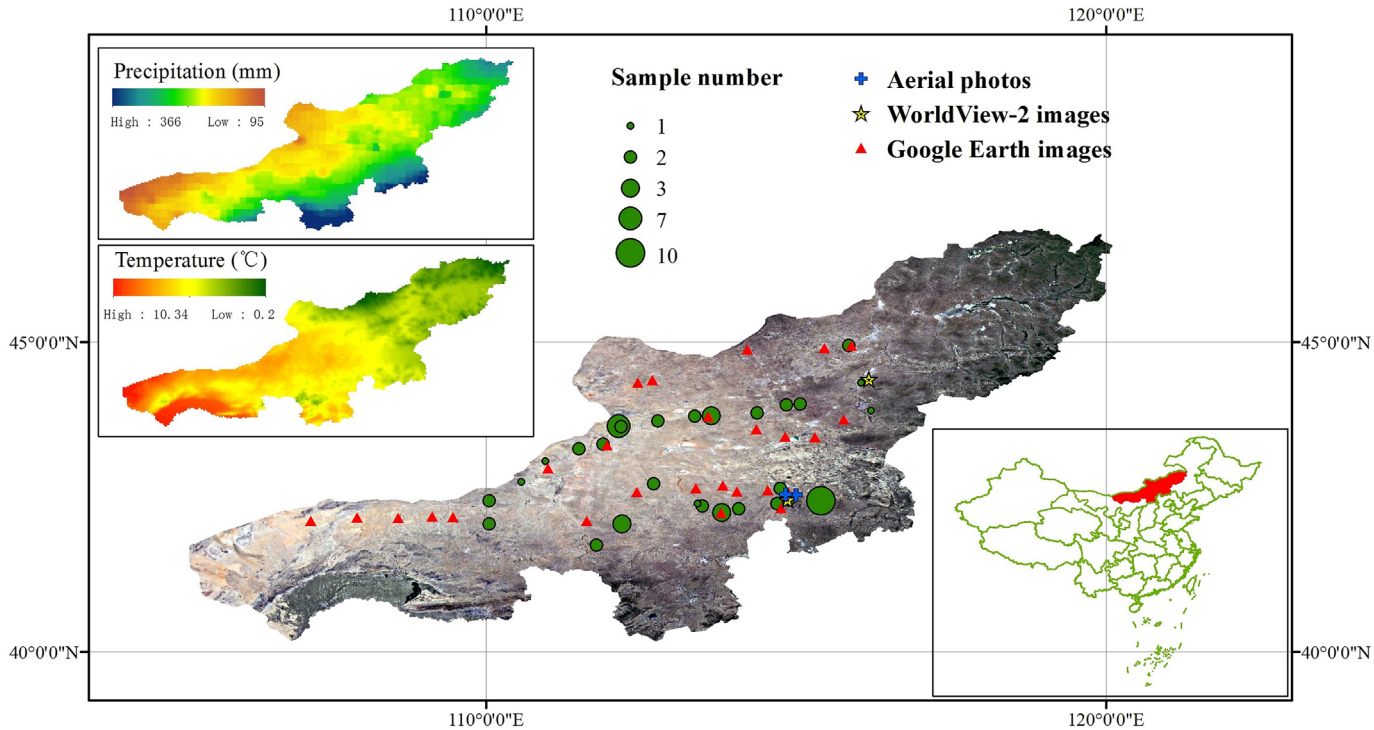

Fig. 1. Study area and location of the field samples and remote sensing images. The study area is in the temperate arid and semiarid grassland in central Inner Mongolia, China. The base map is from Google Earth (GE). The meteorological data in the top left corner indicate the annual average precipitation and temperature. Green circles denote the field sites, and the circle size represents the number of main stem samples. Blue crosses, red triangles, and yellow stars represent the locations of aerial photos (AP), WorldView-2 (WV2) images, and images from GE, respectively. (For interpretation of the references to color in this figure legend, the reader is referred to the web version of this article.)

limited historical data.

2. Study area

The study area is in the temperate arid and semiarid grassland regions of Inner Mongolia, Northern China, which covers the Xilin Gol League and the Ulanqab, Baotou, and Bayan Nur cities (Fig. 1). The dominant leguminous shrubs are *C. microphylla* Lam., *C. korshinskii* Kom., *C. stenophylla* Pojark., and *C. intermedia* Kuang et H. C. Fu. Due to their varied levels of drought tolerance and cold resistance, the shrub crown area also varies with local climatic conditions, including precipitation and temperature (Wang and Ni, 2009). The main herbaceous species in this region are *Leymus chinensis* (Trin.) Tzvel., *Stipa grandis* P. Smirn., *Achnatherum splendens* (Trin.) Nevski, *Cleistogenes squarrosa* (Trin.) Keng, and *Artemisia frigida* Willd. The grass coverage increases from west to east in the study area due to an increasing trend of rainfall.

Meteorological records from 1981 to 2010 show that the mean annual precipitation varied from approximately 100 mm to 360 mm, with nearly 75% occurring from May to October. The mean annual temperature varied from approximately 0 °C to 10 °C, with the maximum occurring in July and the minimum occurring in January (Li et al., 2014). The soil types are chestnut and light chestnut, and the soil textures are primarily sandy and sandy loam. Caliche resulting from dissolved $CaCO_3$ leached by rainwater is common in the soil profile. The study area is primarily used for livestock farming, sometimes leading to severe grassland degradation and vulnerability to shrub expansion (Peng et al., 2013).

3. Data and methods

3.1. Data

3.1.1. Field samples

We surveyed 27 sites in April 2017 along the precipitation gradient from east to west and around the HSR images (Fig. 1), and 67 shrub main stem samples were collected, including *C. microphylla*, *C. stenophylla*, and *C. intermidia*. At each site, we investigated at least two shrubs with different crown sizes. The shrub individuals were cut using a Tajima PUL265-KCH handsaw to ensure smooth sections (Wang et al., 2001). The main stem sample was collected for further analysis in the laboratory. Crown sizes were recorded by measuring the long and short axes of the crown, and then the crown areas were calculated by assuming that the projection of the crown was oval. All sites were established on flat ground or in the middle of gentle slopes to avoid abnormalities in the shrub size caused by micro-topography and spatially heterogeneous rainfall distributions. Large mounds appear around shrub roots due to their high sand-fixing capacity and resistance to wind erosion. The stems are buried below the mounds. These mounds need to be removed before the shrub stem samples could be collected. Approximately 5-cm-long stems were sawed from the shrubs. Regeneration strategies for *Caragana* include seed and clonal reproduction. Therefore, many individuals have more than one main stem or root. In the end, we selected 44 individuals with only one main stem as valid samples.

3.1.2. Metrological data

Annual precipitation data from 1981 to 2010 were used for the regional analysis in this study. This dataset was generated by fitting a partial thin plate smoothing spline with the orography and reanalysis data as explanatory variables to the ground-based observations to estimate a trend surface, and a simple Kriging procedure was then applied

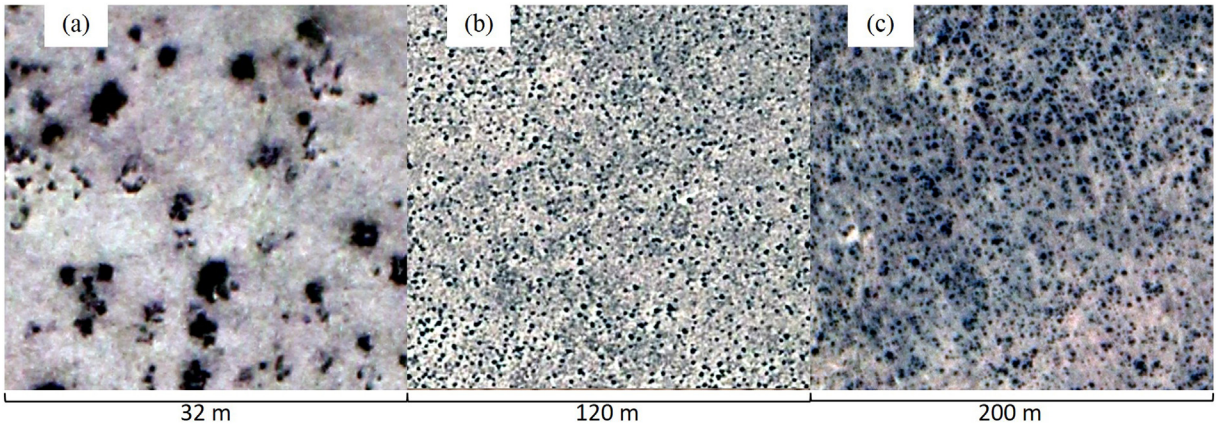

Fig. 2. Examples of remote sensing images (true color) at three different geographic sites: (a) AP image, (b) image from GE, and (c) WV2 image. The size of each snapshot is 400 × 400 pixels.

to the residual for the trend surface correction (Li et al., 2014). Approximately 700 stations over Mainland China were used to produce a dataset with a resolution of 1 km. This dataset has smaller errors than the National Centers for Environmental Prediction (NCEP) Climate Forecast System Reanalysis dataset and the Princeton Global Meteorological Forcing dataset (Li et al., 2014).

3.1.3. Remote sensing data

Caragana grows alone rather than in clumps in the study area (Fig. 2). Therefore, we can use HSR remote sensing images to recognize and identify shrub individuals. Table 1 lists the HSR images used to identify the shrubs.

Aerial remote sensing can achieve a very high spatial resolution. However, applying it over a large spatial area under the restrictions of weather and funding is difficult. Therefore, we acquired only three true color (red, green, blue bands) AP photos with 0.08 m resolution in Zhengxiangbai Banner, Inner Mongolia, in August 2013. Because an increasing number of HSR commercial satellites are being launched, observing the ground surface in detail on a large geographical scale has become feasible. However, HSR is still too expensive to be applied over a large geographical range. Two WV2 images captured in Xilinhot were collected in May and July 2012. The WV2 images have a panchromatic

Table 1
The high spatial resolution remote sensing images used in this study.

Image ID	Longitude	Latitude	Precipitation* (mm y^{-1})	Area (km^2)	Acquisition date	Source**	Spatial resolution** (m)
GE-1	112.45	44.35	146	0.72	2013-4-18	GeoEye-1	0.50
GE-2	112.68	44.38	150	2.25	2013-4-18	GeoEye-1	0.50
GE-3	113.58	43.79	157	1.44	2013-7-20	GeoEye-1	0.48
GE-4	114.05	42.59	209	2.25	2011-6-26	GeoEye-1	0.49
GE-5	113.81	42.68	196	2.25	2011-7-26	WorldView-2	0.46
GE-6	114.88	42.56	243	2.25	2011-6-26	GeoEye-1	0.49
GE-7	114.54	42.60	226	2.16	2011-6-26	GeoEye-1	0.49
GE-8	113.00	43.86	150	2.25	2013-7-20	GeoEye-1	0.48
GE-9	113.40	42.61	188	2.25	2011-9-19	GeoEye-1	0.48
GE-10	112.43	42.57	174	2.25	2011-8-1	GeoEye-1	0.45
GE-11	111.95	43.33	135	2.25	2013-8-25	GeoEye-1	0.45
GE-12	115.76	43.75	213	1.44	2012-5-4	GeoEye-1	0.47
GE-13	115.30	43.46	211	2.25	2012-5-26	GeoEye-1	0.48
GE-14	114.82	43.47	200	0.36	2013-5-20	GeoEye-1	0.49
GE-15	114.36	43.59	180	0.81	2012-10-24	GeoEye-1	0.45
GE-16	114.21	44.88	182	0.5625	2003-8-10	QuickBird-2	0.62
GE-17	115.45	44.90	199	0.81	2010-8-25	GeoEye-1	0.48
GE-18	115.89	44.94	206	0.36	2010-8-25	GeoEye-1	0.48
GE-19	111.00	42.95	151	1.44	2013-12-1	GeoEye-1	0.51
GE-20	107.17	42.11	118	0.405	2012-9-19	GeoEye-1	0.45
GE-21	108.58	42.15	146	0.2025	2013-2-14	GeoEye-1	0.42
GE-22	107.92	42.16	133	0.405	2012-9-19	GeoEye-1	0.50
GE-23	109.13	42.18	155	0.54	2011-10-20	GeoEye-1	0.47
GE-24	111.62	42.11	194	0.54	2013-12-23	GeoEye-1	0.48
GE-25	109.47	42.17	162	0.54	2011-10-20	GeoEye-1	0.47
GE-26	113.78	42.24	215	1.44	2011-9-22	GeoEye-1	0.44
GE-27	114.75	42.31	251	0.405	2011-6-29	GeoEye-1	0.51
AP-1	114.83	42.53	243	0.64	2013-8-5	Aerial image	0.08
AP-2	114.84	42.53	243	0.192	2013-8-5	Aerial image	0.08
AP-3	114.83	42.54	243	0.64	2013-8-5	Aerial image	0.08
WV2-1	114.86	42.45	250	7.76	2012-7-20	WorldView-2	0.50
WV2-2	116.17	44.40	205	2.49	2012-5-12	WorldView-2	0.50

* Precipitation is the average annual value from 1981 to 2010.

** The sources and spatial resolutions for images acquired from GE were provided by DigitalGlobe (https://discover.digitalglobe.com/). Images from GE were downloaded with 0.3 m pixel size.

band with 0.5 m resolution and multispectral bands (Blue, Green, Red, and NIR bands) with 2 m resolution. We pan-sharpened the WV2 images into multispectral images with 0.5 m resolution using the Gram-Schmidt pan-sharpen method in ENVI 5.1 software. Google Earth (GE) provides free access to very high spatial resolution remote sensing images from multiple sources. To acquire images from GE (hereafter GE images), we divided the images into several grids using the grid overlay function in Google Earth 4.3 and captured JPEG images of each square grid with 0.3 m pixel size. Then, a complete image of each study site was reconstructed by mosaicking these JPEG images (Chang et al., 2009). Along the gradient of precipitation, we collected 27 GE images with areas of 0.2–2.25 km^2. Table 1 lists the locations, covered areas, acquisition dates, sources, and spatial resolutions of the remote sensing images. It should be noted that GE images are pan-sharpened true color images. Given the clear color and shape differences between the shrub individuals and the background, even though GE images does not include the near infrared band, this does not affect the identification of individual shrubs.

3.2. Methods

3.2.1. Shrub age determination for the field samples

Shrubs often have no definite annual growth rings (Seligman and Henkin, 2000), and no previous studies have acquired the annual growth rings or have determined the age of *Caragana*. The visibility of ring boundaries can be enhanced by either sanding with grit sandpaper or staining the stem thin sections (Myers-Smith et al., 2015; Schweingruber and Poschlod, 2005). After the known annual ring measurement methods were tested, we were able to observe clear annual growth rings for only 13 samples (Fig. 3).

To reconstruct the ages of the remaining valid shrub samples, we investigated the effect of meteorological factors on the annual growth of a shrub stem. The stem radius was measured by averaging the lengths in two vertical directions for the 13 samples. The number of annual growth rings was counted. We then obtained the average ring width for each sample (Table 2). Regression analysis revealed no obvious positive relationship between the growth ring width and precipitation. This result is consistent with observations of another typical plant in the arid region of Inner Mongolia, namely, *Haloxylon ammodendron* (C. A. Mey.) Bunge, whose stem width is well correlated to the number of growth rings, while the relationship between its stem radial growth rate and precipitation is poor (Wang et al., 2001). As an alternative method, we used the average growth ring width (1.085 mm) to estimate the ages of the remaining shrub samples. The standard deviation of these annual growth ring widths was 0.197 mm.

Table 2
Samples with clear annual growth rings.

Sample ID	Estimated age	Average ring width (mm)	Annual precipitation (mm y^{-1})	Crown area (m^2)
1	19	1.429	205	2.97
2	10	1.400	218	1.32
3	10	1.333	228	1.04
4	8	1.250	183	0.38
5	12	1.125	223	0.95
6	9	1.067	250	0.71
7	11	1.000	122	0.47
8	11	1.000	141	0.95
9	12	1.000	201	0.47
10	9	0.900	183	1.53
11	8	0.900	250	0.27
12	16	0.875	175	0.57
13	8	0.833	122	1.06

Note: The sample age was estimated by dividing the stem radius by the average growth ring width.

3.2.2. Shrub age estimation model

It has been observed that the crown growth of certain shrubs is nearly constant over the lifespan of an individual at a geographical site (Crisp and Lange, 1976; Myers-Smith et al., 2011). Bao et al. (2015a) also found that the crown area of *C. microphylla* is positively linearly correlated with its age. Therefore, we defined the crown growth rate as the increase in the crown area per year ($m^2\,y^{-1}$) and assumed that the crown growth rate of the shrubs is a constant at each geographical site. Several studies have found that the shrub growth rate is related to climatic factors, such as precipitation and temperature (Li et al., 2016; Malkinson and Jeltsch, 2007). We created a shrub age estimation model using the crown area and precipitation while considering rainfall to be the primary constraint of the vegetation growth in arid and semiarid regions (Peng et al., 2014).

At every site, we can obtain

$$S_{i,j} = A_{i,j} \times v_i + e_i, \tag{1}$$

where $S_{i,j}$ is the j-th shrub crown area of age $A_{i,j}$ in site i; v_i is the shrub crown area growth rate ($m^2\,y^{-1}$) at site i; and e_i is the intercept, which denotes an individual's crown area at age 0. Precipitation is the primary constraint of the shrub growth in this region. Therefore, we used a simple linear model to correlate the rainfall and v_i, as shown in Eq. (2).

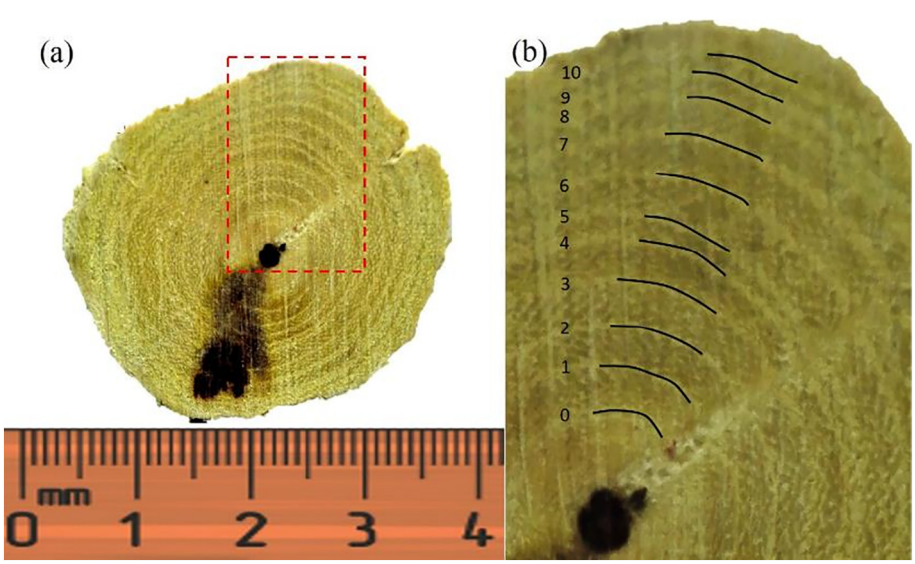

Fig. 3. Shrub stem sample section with annual growth rings: (a) the transect of the main stem sample and (b) an enlarged picture corresponding to the red rectangle in panel (a). The growth rings and years are marked in panel (b). (For interpretation of the references to color in this figure legend, the reader is referred to the web version of this article.)

$$v_i = a_i \times P_i + b_i, \tag{2}$$

where P_i is the annual precipitation (mm y^{-1}) at site i, a_i is the slope, and b_i is the intercept. Eq. (1) implies that e_i may vary by geographical site; therefore, we associated it with precipitation to reduce the number of variables:

$$e_i = c_i \times P_i + d_i, \tag{3}$$

where c_i is the slope and d_i is the intercept. Therefore, the shrub individual age estimation model is expressed as

$$A_{i,j} = \frac{S_{i,j} - (c_i \times P_i + d_i)}{a_i \times P_i + b_i}. \tag{4}$$

We fitted Eq. (4) using 44 valid samples and then removed outliers whose deviations were larger than twice the standard deviation. Among the remaining samples, we randomly selected three quarters of the samples to fit Eq. (4) and kept the rest one quarter for the purpose of cross-validation. The above procedure was repeated 100 times. For comparison, we also estimated the shrub age using only the shrub crown area.

3.2.3. Object-based shrub identification from multiple remote sensing images

The shrub crown area was retrieved from the HSR images. Then, the shrub age was estimated using the method proposed in Section 3.2.2. We used an object-based analysis to identify the shrub individuals in multiple HSR remote sensing images (Table 1). The images were first segmented by a visually optimal scale using the eCognition software with color and smoothness parameters of 0.9 and 0.5, respectively. The shrub individuals were then classified to the right scale level by the following rules: (1) mean brightness value and mean band values, (2) mean difference to brighter neighbors, and (3) roundness and shape index. Rule (1) was the primary feature for distinguishing the dark shrubs from the bright backgrounds. Rule (2) determined the mean layer difference for neighboring objects weighted with respect to the length of the border between the objects. Shrub objects have oval shapes, while other dark patches usually have irregular shapes. Rule (3) uses parameters to describe the shape of an object in order to separate shrubs and other dark patches, such as the tall grass *Achnatherum splendens*.

After the image segmentation and classification, the areas covered by the shrub objects could be calculated according to the number of pixels in every object, which was achieved by converting the raster classification image into vector data using the ArcGIS tools. Then, we obtained the crown size of each individual shrub in the entire image.

Remote sensing images with different spatial resolutions vary in their capabilities to distinguish objects. AP images can detect very small shrubs, whereas GE images with relatively coarse spatial resolution may miss small shrubs. We assessed the resolving power of the GE images because our main data source was GE imagery and the population structure may be influenced by its relatively low spatial resolution (about 0.5 m, see Table 1). We used AP images as the reference data because its spatial resolution is sufficiently high (0.08 m) and it is fairly close to the ground truth. Then, a 1.026 ha region filled with a range of shrub crown sizes and covered by both AP and GE images was selected as the verification plot. However, an evident geometrical position error existed between the AP and GE images. Therefore, a relative geometric correction was conducted with 50 ground control point pairs selected from the images using ENVI. In the end, the root mean square error (RMSE) was 1.56 pixels (0.12 m), which was sufficiently small. Then, shrub individuals were identified from both images. Comparing the classification results of the GE and AP images allowed us to evaluate the shrub identification accuracy of the GE images. A few clumping shrubs that could not be separated due to the excessively narrow distance between the shrubs; these shrubs were removed before comparing the shrub areas identified from the AP and GE images.

3.2.4. Shrub population structure model

A negative exponential distribution was found to be more suitable than the power function model for describing the decline in the shrub density with aging (Kuuseoks et al., 2001) due to the constant mortality rate in the selected shrub population (Dahlgren et al., 2016). The negative exponential model is

$$Y_{ij} = Y_{0j} e^{-b_j X_{ij}} \varepsilon_{ij}, \tag{5}$$

where Y_{ij} is the proportion of shrubs with age i-class in plot j, Y_{0j} is the proportion of shrubs with age 0 in plot j, e^{-b_j} is the survival rate, X_{ij} is the age i-class in plot j, and ε_{ij} is the error term. The logarithmic transformation of Eq. (5) is

$$\ln Y_{ij} = \ln Y_{0j} - b_j X_{ij} + \varepsilon_{ij}, \tag{6}$$

where the slope b_j represents individual losses due to mortality, the intercept indicates the annual input of individuals into the age 0-class, and Y_{0j} is the regeneration count (i.e., the annual input of shrubs into the 0 year age-class).

The number of shrub individuals should decrease with aging (Dahlgren et al., 2016). However, small shrubs might be captured by remote sensing sensors due to the limitations in the sensor resolving power and the segmentation algorithm. Therefore, the count of small shrubs is fewer than the actual number of small shrubs, resulting a large degree of uncertainty in the negative exponential model fitting. To ensure a better performance, we fitted this model from the highest shrub proportion point for every study site (Fig. 4).

4. Results

4.1. Shrub age determination for the field samples

The average growth ring width, which is equal to the stem radius divided by the number of growth rings, is 1.085 mm for the 13 samples. The average absolute deviation in the ages of the samples is 1.82 y between the number of annual growth rings and the estimated age. We estimated the ages of all the shrub samples using the average growth ring width.

We fitted Eq. (4) using the MATLAB curve fitting tools. After removing four samples that had errors larger than twice the standard deviation (6 y) of the shrub age error, the resulting RMSE is 2.202 and the coefficient of determination (R^2) is 0.716 (the adjusted R^2 is 0.692, as shown in Eq. (7)). Meanwhile, the R^2 of the shrub crown area and the shrub age is 0.656 (Fig. 5a). This result suggests that precipitation can enhance the accuracy of the shrub age estimation model (Fig. 5b). In the cross-validation experiment, we repeated 1000 experiments with 30 samples for training and 10 samples for testing and obtained a final average RMSE of 2.0662.

$$A_{i,j} = \frac{S_{i,j} - (1.083 - 0.009614 \times P_{i,j})}{0.0009707 \times P_{i,j} - 0.04573}. \tag{7}$$

4.2. Shrub individual identification via remote sensing images

The shrub individuals were identified via an object-based analysis from multiple HSR remote sensing images (Fig. 6). Visually inspecting the results indicates that the shrub individuals were identified in a satisfactory manner. However, certain shrubs were too small to be precisely captured by images or to be identified by eCognition, and a few clumping shrubs could not be separated because they were too close to each other.

To evaluate the capture capacity of the small shrubs using GE images, we examined shrub identifications of AP and GE images at the same location (Fig. 7). The omission errors of the GE image (the red points in Fig. 8(a)) were primarily shrubs with crown areas of less than 1.5 m^2 (Fig. 8(b)). Only 37.4% of the shrubs smaller than 1.5 m^2 were

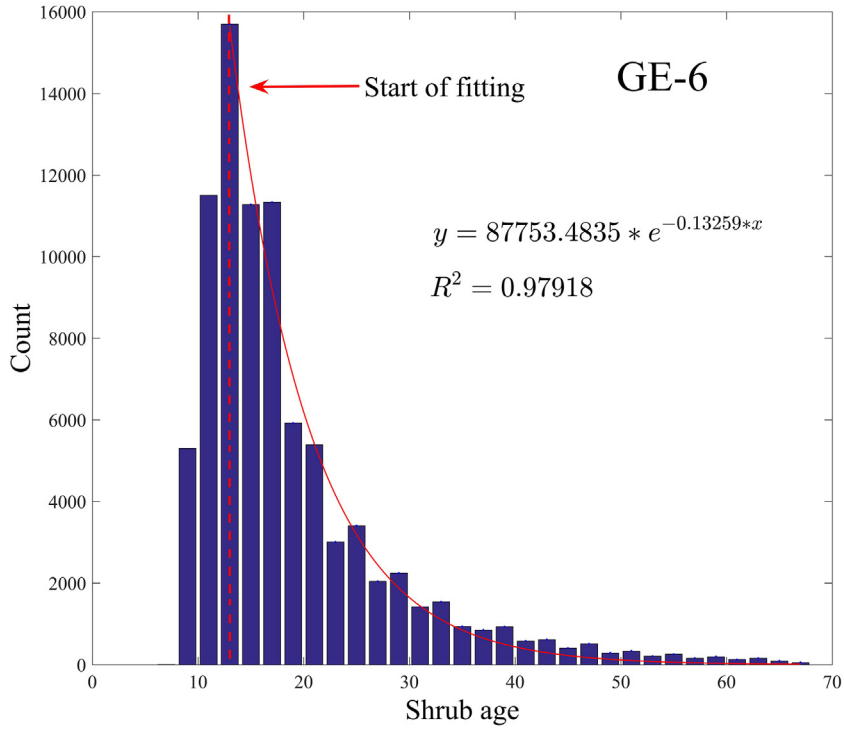

Fig. 4. Model fitting of the population structure.

detected in the GE image, whereas over 99% of the shrubs larger than 1.5 m^2 were detected. Furthermore, small shrubs had larger errors than big shrubs (green boxes in Fig. 8a). The average absolute errors of the shrubs smaller than 1.5 m^2 and those larger than 1.5 m^2 were 51.8% and 25.4%, respectively. A 1.5 m^2 area is approximately as large as a box measuring 4 × 4 GE pixels, which corresponds to a shrub individual that is approximately 16 years old. Moreover, the crown size of shrub individuals tended to be underestimated in the AP images. In cases where sub-objects merge into shrub objects, areas with light-colored pixels at the edges of shrubs are often missed because the outer layers of shrub objects contain lighter-colored pixels than those in the interior (Laliberte et al., 2004).

4.3. Error analysis for the shrub age estimation model

In the proposed shrub age estimation model, two factors influence the accuracy of the age estimation, i.e., the precipitation error and the shrub crown area measurement error. Under a given shrub crown area of 2 m^2 and a precipitation of 200 mm y^{-1}, we simulated the shrub age estimation error derived from the precipitation error (Fig. 9a). The result indicates that the precipitation error can nonlinearly affect the shrub age estimation accuracy; the shrub age estimation errors range from 1.8 y to 1.3 y when the precipitation errors vary within ± 25 mm y^{-1}. Considering a shrub crown area of 2 m^2 at a precipitation of 200 mm y^{-1}, the estimated shrub age is approximately 19.1 y, suggesting that the shrub age estimation is not greatly affected by the

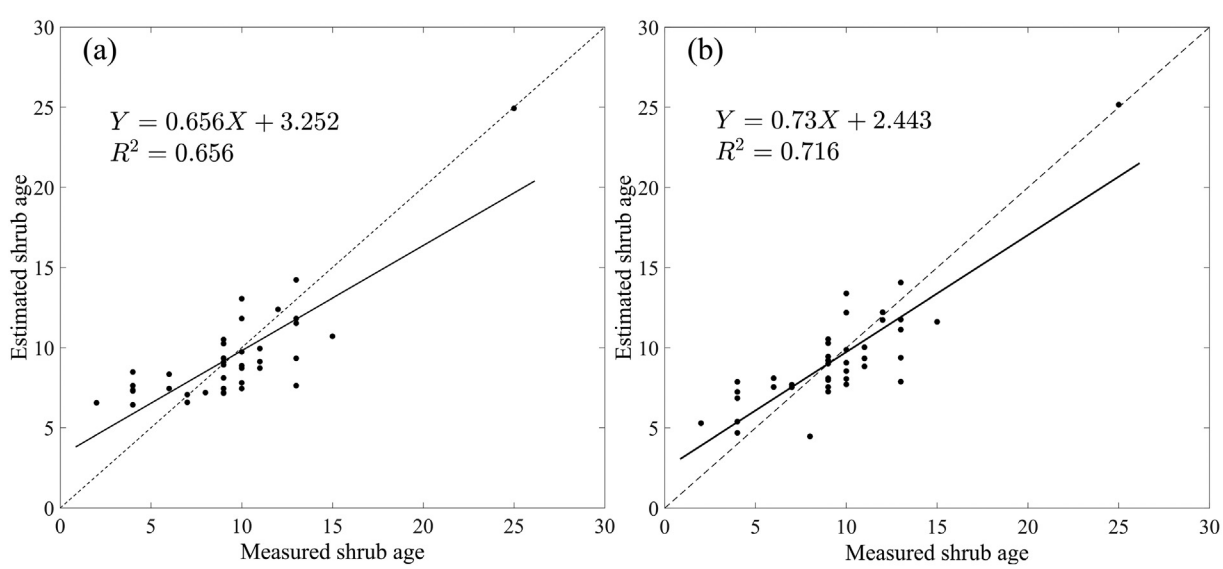

Fig. 5. Linear relationship between the measured and estimated shrub ages: (a) using only the shrub crown area and (b) using the shrub crown area and the precipitation estimation model.

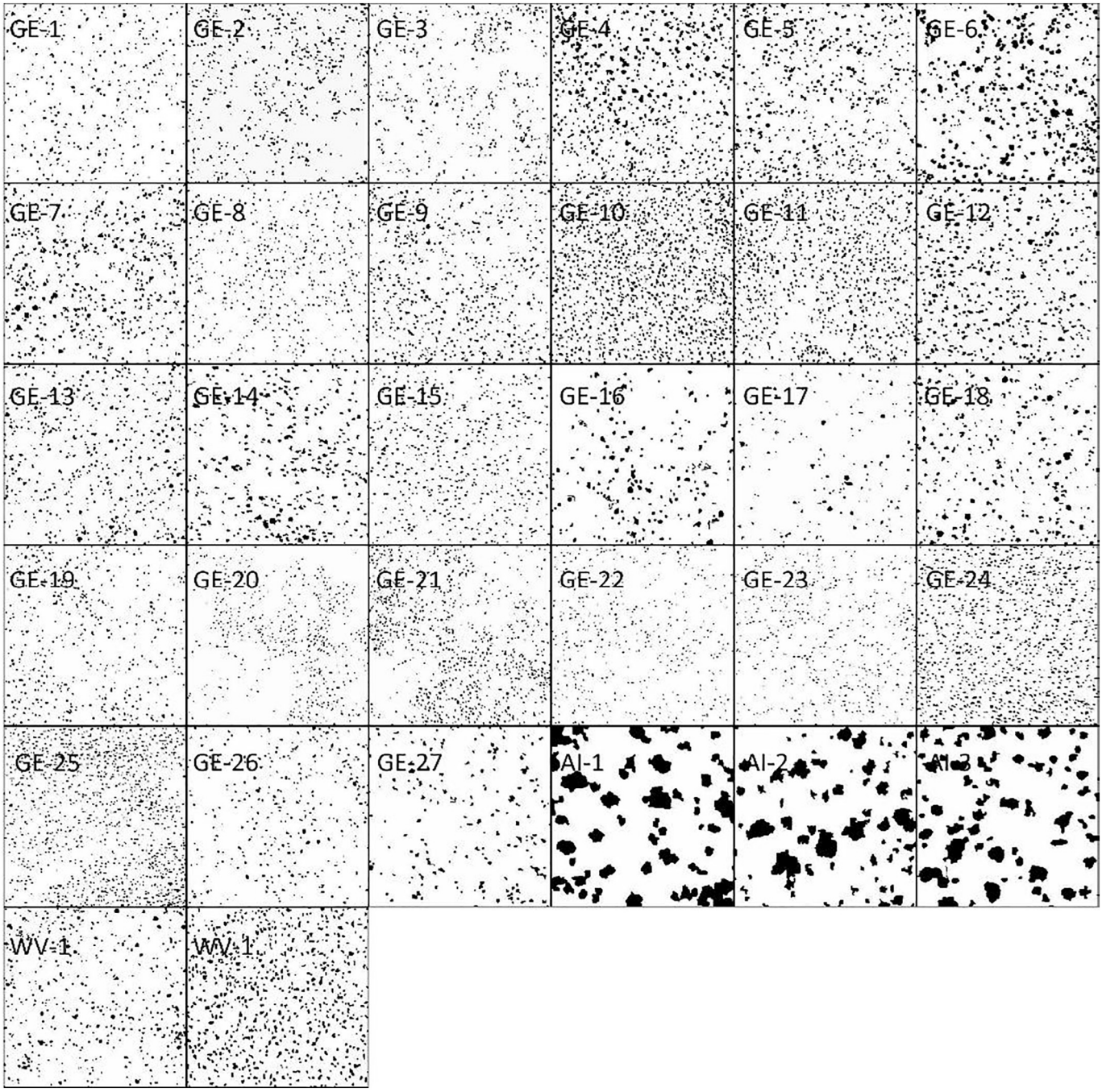

Fig. 6. Individual shrub identification results. Black blocks are shrubs, and white indicates the background. The size of each snapshot is 400 × 400 pixels (GE images: 120 m × 120 m, AP images: 32 m × 32 m, and WV2 images: 200 m × 200 m).

precipitation error.

According to Eq. (7), we can obtain the relative shrub age estimation error caused by the shrub area measurement error:

$$\frac{\Delta A}{A} = \frac{\Delta S}{S - (1.083 - 0.009614 \times P_i)}, \tag{8}$$

where ΔA is the shrub age estimation error caused by the shrub crown area measurement error, which can be obtained from the difference between the ages retrieved from the AP and GE images (Fig. 7); A is the shrub age estimated from the AP image; ΔS is the shrub crown area measurement error, which is the difference between shrub crown areas measured from the AP and GE images; S is the shrub crown area measured from the AP image; and P_i is the annual precipitation at site i, which here is 243 mm y^{-1} according to the AP and GE image location.

According to Eq. (8), we can draw a scatter plot to describe the distribution of the shrub age relative error induced by the crown area measurement error (Fig. 9b). We find that the shrub age relative error tends to gradually decrease with an increasing shrub crown area, even though the number of samples with areas larger than 5 m^2 is small. The relative age estimation errors are very large for small crown areas; however, the number of overestimates and underestimates are nearly identical. The evidence from the AP and GE images suggests that the shrub age estimation error caused by the crown area measurement error might not affect the population structure model fitting.

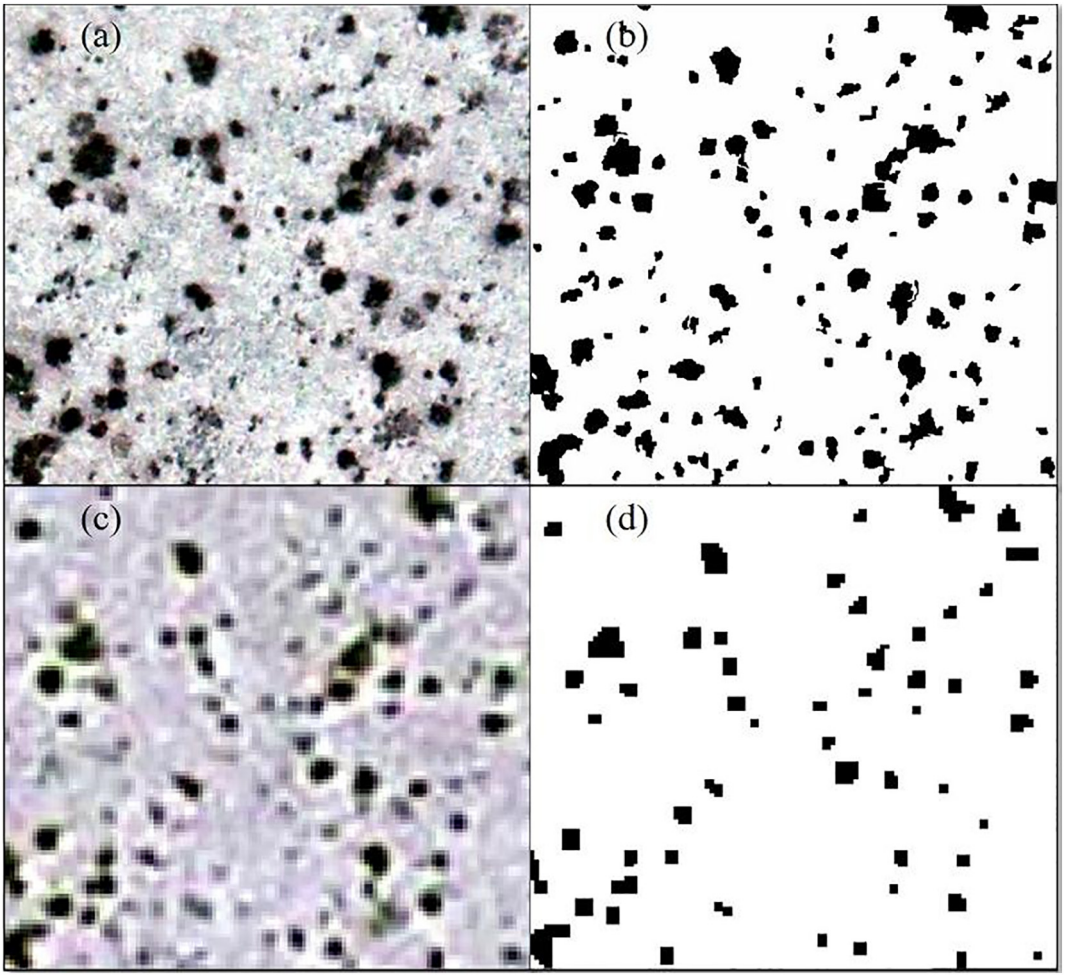

Fig. 7. Resolving power of AP and GE images: (a) AP image, (b) the shrub identification result of panel (a), (c) GE image of the same area as in panel (a) but resampled to 0.08 m resolution, and (d) the shrub identification result of panel (c).

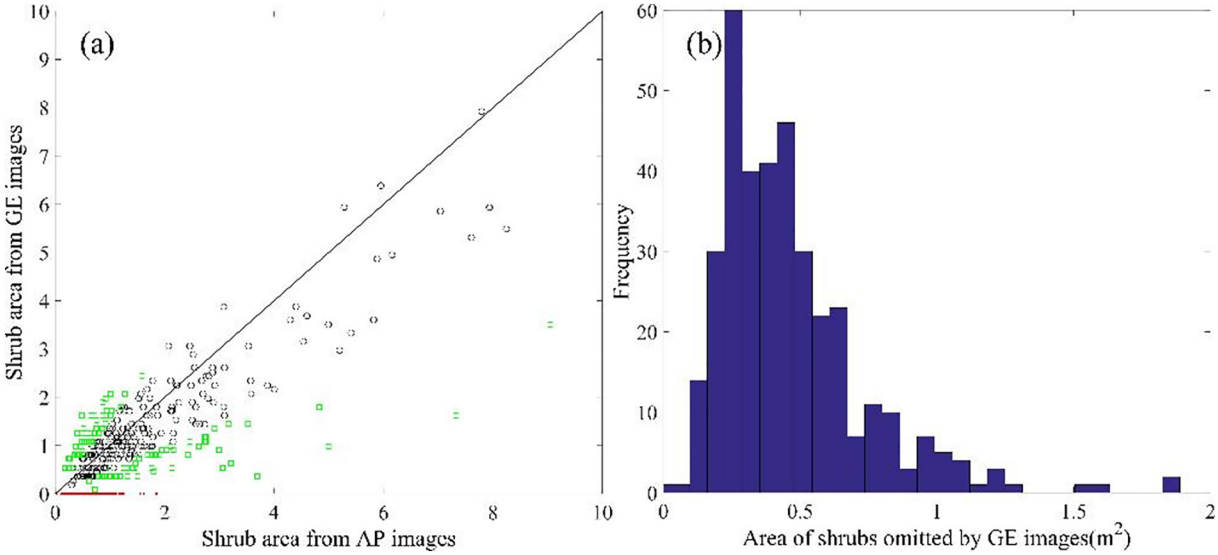

Fig. 8. Comparison between the shrub area extraction from the AP and GE images: (a) shrub area (m^2) difference between the AP and GE images and (b) area distribution of shrubs that failed to be detected by the GE image. The black circles represent shrubs that were detected by both images and their relative errors were less than 50%. The green boxes represent shrubs that were detected by both images and their relative errors were greater than 50%. The red points represent the shrubs missed by the GE image but were detected by the AP image. (For interpretation of the references to color in this figure legend, the reader is referred to the web version of this article.)

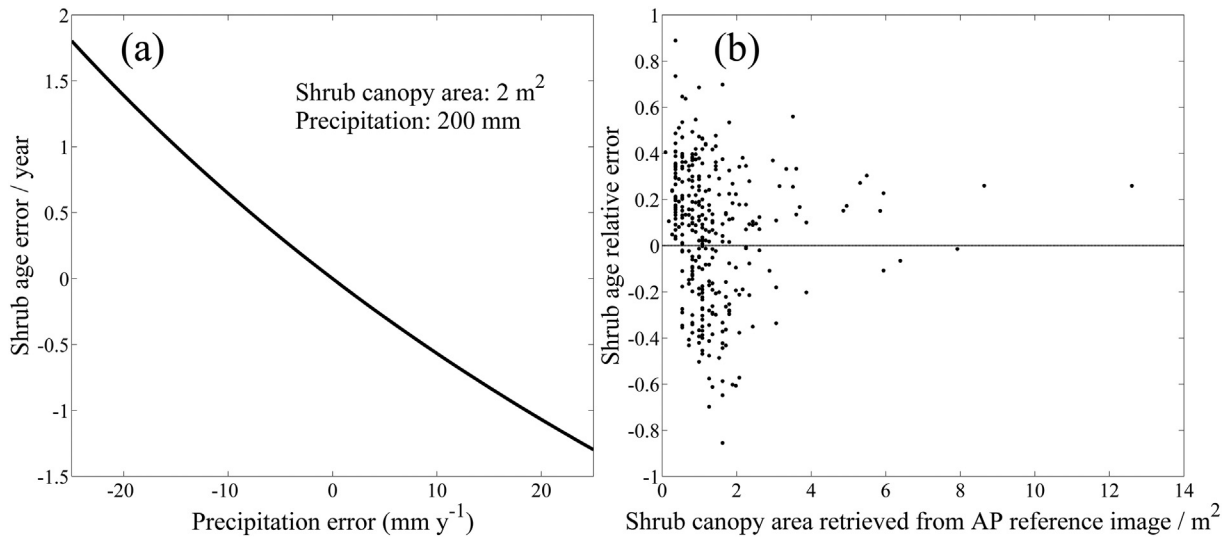

Fig. 9. The shrub age estimation error affected by (a) the precipitation error and (b) the shrub crown measurement error.

4.4. Population structure and dynamics

Fig. 10 shows the population structure and fitting results of all 32 images. Nearly all coefficients of determination were larger than 0.9 except for GE-20, which had the least precipitation. Shrubs in GE-20 were too small to be identified precisely, and large errors in the age estimation may lead to the inaccurate fitting in the negative exponential model. The average regeneration count and survival rate of all the study sites were 564 N/ha (i.e., Y_0 divided by the plot area) and 0.87, respectively, which means that 564 seedlings per hectare would emerge by seed or sprout from surviving meristems, whereas 13% of the population would disappear due to ecological factors, such as population competition.

Fig. 11 shows the geographic distribution of the survival rate and regeneration count per hectare. The shrub populations in the middle and western portions of the study region had a low survival rate (Fig. 11a), which indicates that strong competition may exist in these areas due to low precipitation or high shrub density. However, the regeneration count did not show an obvious distribution pattern (Fig. 11c). By dividing these areas into three groups according to the precipitation gradients of 100–150 mm y^{-1}, 150–200 mm y^{-1}, and 200–250 mm y^{-1}, we observed that the survival rate tended to increase with precipitation (Fig. 11b), whereas the regeneration count had no such a trend (Fig. 11d).

5. Discussion

(1) Shrub sample measurement

The ideal method for determining the age of a shrub sample is to count the number of annual growth rings. However, only 13 samples had distinct annual growth rings. The mean annual growth ring width, with an absolute error of 1.82 y, was therefore used to estimate the ages of the field samples. However, this method may not work well for excessively large shrubs due to the lack of big shrub samples. In addition, field sampling was conducted in April, before the shrubs turned green. The crown area might therefore be slightly smaller than the crown areas in summer when the remote sensing images were acquired due to branches perishing and slight grazing in winter. Therefore, using the crown area detected by the remote sensing images might overestimate the shrub age. Shrub age measurements with improved precision require additional samples with clear annual growth rings and field sampling during the summer.

(2) Feasibility of the shrub age estimation model

We proposed a new shrub age estimation model using the image-based shrub crown area and precipitation. This model has a direct physical explanation and performs better than a method that uses only the shrub crown area. Different precipitation levels lead to various mean crown growth rates of the shrubs. Eqs. (2) and (7) imply that the large precipitation stimulates quick shrub growth, drawing a conclusion consistent with previous research (Li et al., 2016; Malkinson and Jeltsch, 2007). With precipitation decreasing from 250 mm y^{-1} to 117 mm y^{-1}, the crown growth rate of the shrubs decreased from 0.197 m^2 y^{-1} to 0.0679 m^2 y^{-1}, which is comparable to the behavior of *C. microphylla* in Horqin Sandy Land (Bao et al., 2015a). With the decrease in precipitation, the initial modeled shrub crown area decreased from -0.042 m^2 to -1.32 m^2. Negative values indicate slow growth at the beginning of life for two possible reasons. The first possibility is that the primary regeneration method of *C. microphylla* and *C. stenophylla* is clonal proliferation from meristems in old shrubs (Liu, 2011; Qiu et al., 2012), which needs to accumulate adequate nutrition before sprouting. The second possibility is that *C. intermedia* regenerates via seed propagation (Zhao and Ren, 2005). Therefore, roots grow quickly in the first two or three trophophase years while the aboveground biomass increases slowly. After this period, ramifications diverge from the roots and the shrub develops a crown (Niu, 2013). In addition, *C. intermedia* grows more quickly than *C. microphylla* during the seedling period (Wu et al., 2016), which is consistent with our result. Climate factors, such as rainfall and temperature, control the distribution and morphology of the *Caragana* genus. *C. microphylla* is distributed in the eastern region of Inner Mongolia and has a larger crown than other *Caragana*. Conversely, *C. intermedia* and *C. stenophylla* are distributed further west and have smaller canopies than our study subject (Wang and Ni, 2009). Even though multiple species were included in the sampling of the *Caragana* genus, they were all in line with the growth function.

This model could be employed to estimate ages of other plant species. However, there are two important preconditions to apply this model to different ecosystems: (1) the plants or patches need to be spatially isolated and (2) there needs to be an evident relationship between age and plant morphology. The limiting factors for plant growth, such as temperature and precipitation, need to be considered in the plant age estimation model. Another problem for the feasibility of such a model is the relationship between the plant crown areas and the resolving power of HSR images. GE provides global HSR observations with free access; however, shrubs crowns smaller than 1.5 m^2 cannot be accurately identified by the GE images in this study. Plants with small

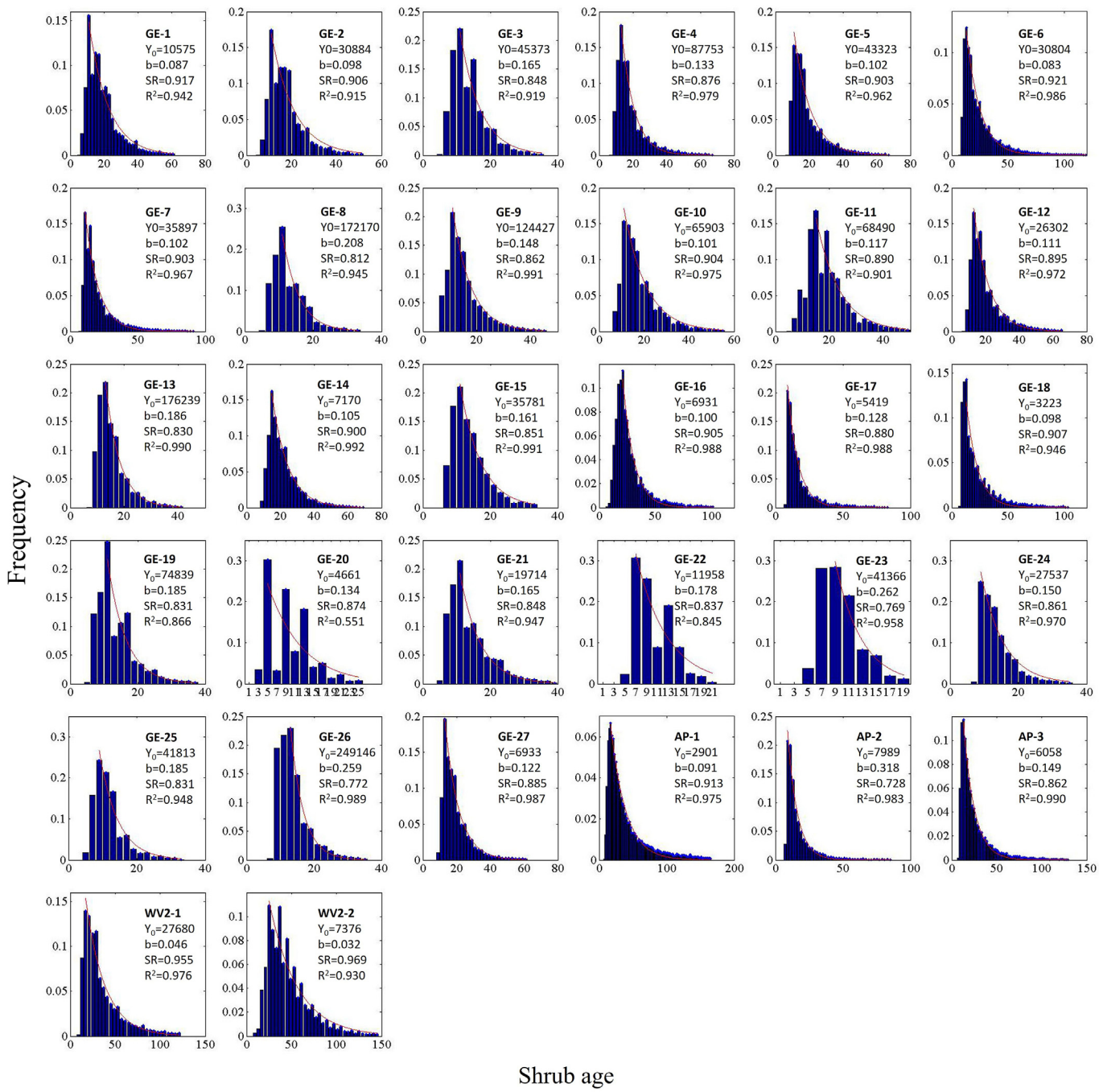

Fig. 10. Population structure fitting result of each site. Y_0 and b are the regeneration count and the mortality factor, respectively, as shown in Eq. (5). SR presents the survival rate e^{-b_j}. R^2 is the goodness of fit.

crown areas require higher spatial resolution data.

(3) Population structure fitting

Remote sensing sensors vary by their resolving power. AP imagery can capture smaller shrubs than GE and WV2 imagery, which means that the start of fitting (Fig. 4) is close to zero, therefore leading to a good fitting of the negative exponential equation and improved parameters, especially the regeneration count. Besides, larger shrub crown areas have lower relative errors. Due to the slow growth rate of shrubs in arid and semiarid regions and the discreteness of the shrub area extracted from remote sensing images, certain age classes were absent. Therefore, we established a histogram of the population structure using a two-year interval (Fig. 4). Consequently, nearly every negative exponential function was fitted perfectly. Population structure provides a conceivable way to study the factors that influence the shrub encroachment process. Since the effect of topography and grazing pressure on the shrub population structure cannot be ignored (Li et al., 2015; Soliveres and Eldridge, 2014), a single population structure cannot represent the local regeneration and survival rates corresponding to the soil and climate conditions. Regeneration estimates are also affected by omitting the young seedlings. In addition, Y_0 is just an estimated value and is not a real birth rate. Results also indicate that the survival rate increases with rainfall, which might indicate reduced competition between shrub individuals at higher levels of rainfall.

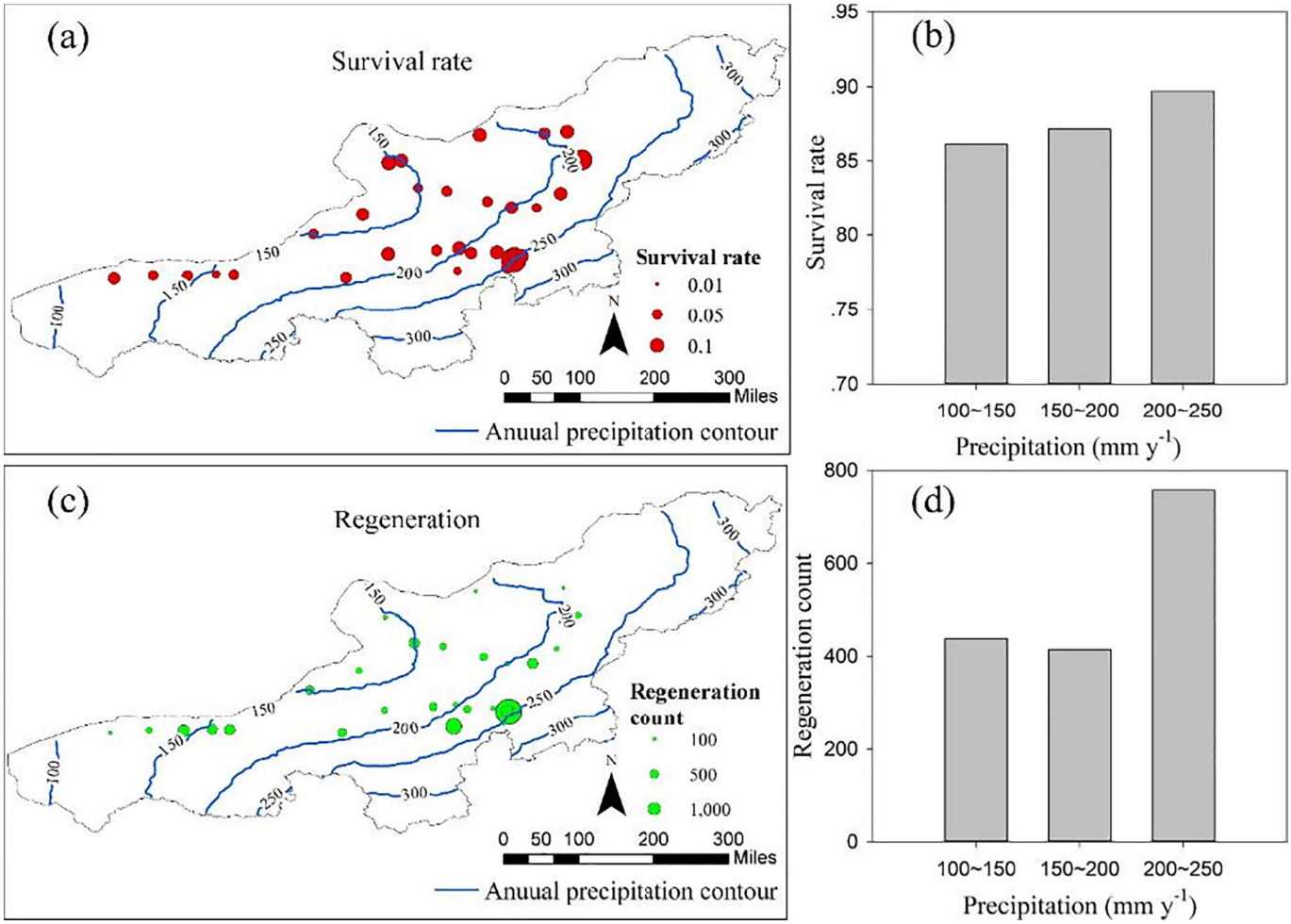

Fig. 11. Distribution of the survival rate and regeneration count over space plotted with the precipitation gradient: (a) geographic distribution of the survival rate, (b) average survival rate for a given precipitation gradient, (c) geographic distribution of the regeneration count per hectare, and (d) average regeneration count per hectare for a given precipitation gradient.

(4) Implications for the shrub encroachment process

Historical perspectives increase our understanding of the population dynamics in the past and provide a reference framework for assessing future patterns and processes (Swetnam et al., 1999). Population structure also involves historical information concerning shrubs; for example, the maximum age reveals the duration of the shrub encroachment (Myers-Smith et al., 2011). The historical shrub expansion speed (i.e., the annual shrub coverage increment) can be calculated from the current shrub coverage divided by the maximum shrub age for each site, assuming that the maximum shrub age represents the initiation date of the shrubs (Myers-Smith et al., 2011). The shrub coverage at each site was acquired via the total crown area divided by the area of the HSR image. According to Eq. (7), the shrub with the largest crown area has the longest growth time. We calculated the average age of the shrubs with the largest 1% of the crown areas to avoid uncertainties in identifying shrub individuals. To reveal the spatial heterogeneity of the past shrub encroachment process, we categorized the shrub coverage increment per year according to precipitation levels of 100–150 mm y^{-1}, 150–200 mm y^{-1}, and 200–250 mm y^{-1} (Fig. 12a). Areas with higher precipitation contain shrubs that expand faster. The past shrub expansion speed depends on the initiation date of the first shrub emergence; however, an HSR image from a single date cannot guarantee that the largest crown marks the first shrub emergence due to mortality. Multi-year observations can be used to reconstruct the past shrub expansion speed and correct the results of this study.

The population structure model can reflect the population dynamics, e.g., regeneration represents the number of new shrubs, and the survival rate estimates the remaining number of new shrubs per year. The product of the regeneration count per hectare and the survival rate, denoted as the new survival count, can be used to predict the shrub development in the next year. We calculated the new survival count of the next year for each site, and averaged them into three groups according to the precipitation levels (Fig. 12b). Fig. 12(b) indicates that areas with higher precipitation have higher levels of new shrub regeneration in the next year. The above preliminary analysis suggests the potential of using population structure models to understand the shrub encroachment process in the past and future.

6. Conclusions

Shrub encroachment in arid and semiarid grasslands marks a transition in the competitive advantages between shrubs and grasses. The monitoring of the shrub encroachment can be achieved via long-term field observations or remote sensing images. This study proposed a new shrub age estimation model and established the population age structure of shrubs for different geographic locations based on the field-surveyed shrub age and its relationship with the crown area and precipitation. The new shrub age estimation method presented in this study considers different crown growth rates affected by different precipitation regimes. This method is suitable for shrubs in arid and semiarid regions in Inner Mongolia, China, and could be extended to

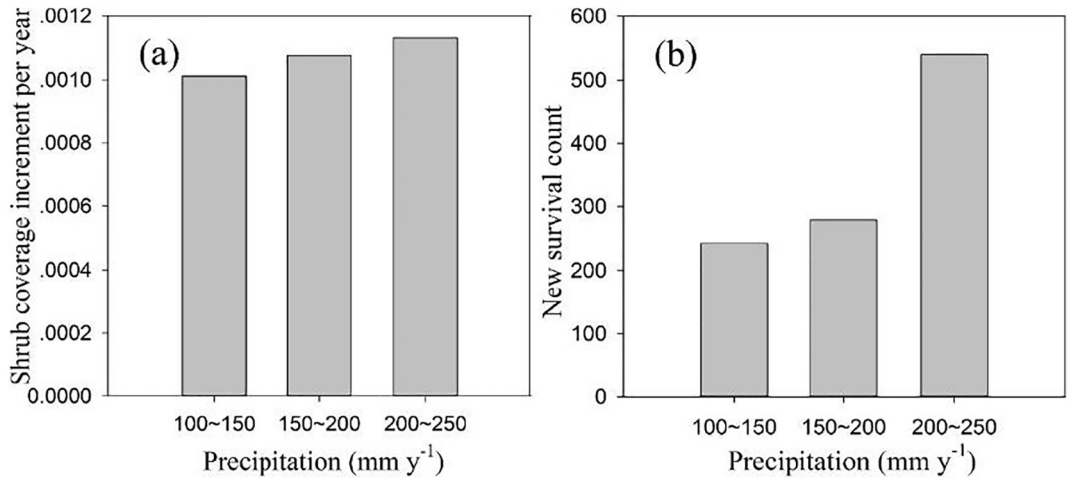

Fig. 12. The shrub encroachment process in the past or future: (a) past shrub expansion speed and (b) new survival count in the next year.

other shrub species in other world regions. On the basis of the crown area detected by HSR remote sensing images and the shrub age estimation model, a shrub age histogram was acquired for each image. Then, a precise population structure, which can be used to assess the population regeneration and survival rates, was established. The shrub population structure constructed on the basis of the remote sensing data can help us understand the process of shrub encroachment in arid and semiarid grasslands and might predict the development and trends of shrub encroachment under future climate scenarios.

Acknowledgement

This work was supported by the National Natural Science Foundation of China (41571406), the Fund for Creative Research Groups of National Natural Science Foundation of China (41621061), and the State Key Laboratory of Earth Surface Processes and Resource Ecology at Beijing Normal University (2015-ZDTD-011). The soil data set is provided by Data Center for Resources and Environmental Sciences, Chinese Academy of Sciences (RESDC) (http://www.resdc.cn).

References

Bao, H., A, L., Feng, J., Mang, L., Liu, D., Jiang, P., 2015a. Population traits of planted *Caragana microphylla* of different ages and its growth after cutting in the Horqin Sandy Land. J. Desert Res. 35, 1527–1531. https://doi.org/10.7522/j.issn.1000-694X.2015.00159. (In Chinese).

Bao, S., Yang, J., Zhao, L., Zhang, P., Niu, Y., Ying, H., 2015b. Genetic diversity of *Caragana microphylla* and *Caragana intermedia* in Inner Mongolia Plateau. Acta Botan. Boreali-Occiden. Sin. 35, 1998–2006. https://doi.org/10.7606/j.issn.1000-4025.1015.10.1998. (In Chinese).

Belsky, A.J., 1992. Effects of grazing, competition, disturbance and fire on species composition and diversity in grassland communities. J. Veg. Sci. 3, 187–200. https://doi.org/10.2307/3235679.

Brotherson, J.D., Davis, J.N., Greenwood, L., 1980. Diameter-age relationships of two species of mountain mahogany. J. Range Manag. 33, 367–370.

Büntgen, U., Hellmann, L., Tegel, W., Normand, S., Myers-Smith, I., Kirdyanov, A.V., Nievergelt, D., Schweingruber, F.H., 2015. Temperature-induced recruitment pulses of Arctic dwarf shrub communities. J. Ecol. 103, 489–501. https://doi.org/10.1111/1365-2745.12361.

Cabral, A.C., De Miguel, J.M., Rescia, A.J., Schmitz, M.F., Pineda, F.D., 2003. Shrub encroachment in Argentinean savannas. J. Veg. Sci. 14, 145–152. https://doi.org/10.1111/j.1654-1103.2003.tb02139.x.

Chang, A.Y., Parrales, M.E., Jimenez, J., Sobieszczyk, M.E., Hammer, S.M., Copenhaver, D.J., Kulkarni, R.P., 2009. Combining google earth and GIS mapping technologies in a dengue surveillance system for developing countries. Int. J. Health Geogr. 8, 1–11. https://doi.org/10.1186/1476-072X-8-49.

Chen, X., Chen, J., Jia, X., Somers, B., Wu, J., Coppin, P., 2011. A quantitative analysis of virtual endmembers' increased impact on the collinearity effect in spectral unmixing. IEEE Trans. Geosci. Remote Sens. 49, 2945–2956. https://doi.org/10.1109/TGRS.2011.2121073.

Chopping, M., 2011. CANAPI: canopy analysis with panchromatic imagery. IEEE Geosci. Remote Sens. Lett. 2, 21–29. https://doi.org/10.1080/01431161.2010.486805.

Chopping, M., Su, L., Rango, A., Martonchik, J., Peters, D., Laliberte, A., 2008. Remote sensing of woody shrub cover in desert grasslands using MISR with a geometric-optical canopy reflectance model. Remote Sens. Environ. 112, 19–34. https://doi.org/10.1016/j.rse.2006.04.023.

Cipriotti, P.A., Aguiar, M.R., 2012. Direct and indirect effects of grazing constrain shrub encroachment in semi-arid Patagonian steppes. Appl. Veg. Sci. 15, 35–47. https://doi.org/10.1111/j.1654-109X.2011.01138.x.

Crisp, M.D., Lange, R.T., 1976. Age structure, distribution and survival under grazing of the arid-zone shrub *Acacia burkittii*. Oikos 27, 86–92.

Dahlgren, J.P., Rizzi, S., Schweingruber, F.H., Hellmann, L., Buntgen, U., 2016. Age distributions of Greenlandic dwarf shrubs support concept of negligible actuarial senescence. Ecosphere 7, 1–6. https://doi.org/10.1002/ecs2.1521.

D'Odorico, P., Fuentes, J.D., Pockman, W.T., Collins, S.L., He, Y., Medeiros, J.S., DeWekker, S., Litvak, M.E., 2010. Positive feedback between microclimate and shrub encroachment in the northern Chihuahuan desert. Ecosphere 1, 1–11. https://doi.org/10.1890/ES10-00073.1.

D'Odorico, P., Okin, G.S., Bestelmeyer, B.T., 2012. A synthetic review of feedbacks and drivers of shrub encroachment in arid grasslands. Ecohydrology 5, 520–530. https://doi.org/10.1002/eco.259.

Duchesne, R.R., Chopping, M.J., Tape, K.D., 2016. Capability of the CANAPI algorithm to derive shrub structural parameters from satellite imagery in the Alaskan Arctic. Polar Rec. 52, 124–133. https://doi.org/10.1017/S0032247415000509.

Eldridge, D.J., Bowker, M.A., Maestre, F.T., Roger, E., Reynolds, J.F., Whitford, W.G., 2011. Impacts of shrub encroachment on ecosystem structure and functioning: towards a global synthesis. Ecol. Lett. 14, 709–722. https://doi.org/10.1111/j.1461-0248.2011.01630.x.

Gang, C., Zhou, W., Chen, Y., Wang, Z., Sun, Z., Li, J., Qi, J., Odeh, I., 2014. Quantitative assessment of the contributions of climate change and human activities on global grassland degradation. Environ. Earth Sci. 72, 4273–4282. https://doi.org/10.1007/s12665-014-3322-6.

Han, Y., Niu, J., Zhang, Q., Dong, J., Zhang, X., Kangsarula, 2014. The changing of vegetation pattern and its driven forces of grassland in Xilin River Basin in thirty years. Chin. J. Grassl. 36, 70–77 (In Chinese).

He, Y., D'Odorico, P., De Wekker, S.F.J., Fuentes, J.D., Litvak, M., 2010. On the impact of shrub encroachment on microclimate conditions in the northern Chihuahuan desert. J. Geophys. Res. Atmos. 115, 1–10. https://doi.org/10.1029/2009JD013529.

Huenneke, L.F., Anderson, J.P., Remmenga, M., Schlesinger, W.H., 2002. Desertification alters patterns of aboveground net primary production in Chihuahuan ecosystems. Glob. Chang. Biol. 8, 247–264. https://doi.org/10.1046/j.1365-2486.2002.00473.x.

Isaacson, S., Ephrath, J.E., Rachmilevitch, S., Maman, S., Ginat, H., Blumberg, D.G., 2017. Long and short term population dynamics of acacia trees via remote sensing and spatial analysis: case study in the southern Negev Desert. Remote Sens. Environ. 198, 95–104. https://doi.org/10.1016/j.rse.2017.05.035.

Kéfi, S., Rietkerk, M., Alados, C.L., Pueyo, Y., Papanastasis, V.P., ElAich, A., de Ruiter, P.C., 2007. Spatial vegetation patterns and imminent desertification in Mediterranean arid ecosystems. Nature 449, 213–217. https://doi.org/10.1038/nature06111.

Kuuseoks, E., Dong, J., Reed, D., 2001. Shrub age structure in northern Minnesota aspen stands. For. Ecol. Manag. 149, 265–274. https://doi.org/10.1016/S0378-1127(00)00559-4.

Laliberte, A.S., Rango, A., Havstad, K.M., Paris, J.F., Beck, R.F., McNeely, R., Gonzalez, A.L., 2004. Object-oriented image analysis for mapping shrub encroachment from 1937 to 2003 in southern New Mexico. Remote Sens. Environ. 93, 198–210. https://doi.org/10.1016/j.rse.2004.07.011.

Levick, S.R., Rogers, K.H., 2011. Context-dependent vegetation dynamics in an African savanna. Landsc. Ecol. 26, 515–528. https://doi.org/10.1007/s10980-011-9578-2.

Li, J., Okin, G.S., Alvarez, L., Epstein, H., 2008. Effects of wind erosion on the spatial heterogeneity of soil nutrients in two desert grassland communities. Biogeochemistry 88, 73–88. https://doi.org/10.1007/s10533-008-9195-6.

Li, T., Zheng, X., Dai, Y., Yang, C., Chen, Z., Zhang, S., Wu, G., Wang, Z., Huang, C., Shen,

Y., Liao, R., 2014. Mapping near-surface air temperature, pressure, relative humidity and wind speed over mainland China with high spatiotemporal resolution. Adv. Atmos. Sci. 31, 1127–1135. https://doi.org/10.1007/s00376-014-3190-8.1.

Li, Q., Jia, Z., Zhu, Y., Wang, Y., Li, H., Yang, D., Zhao, X., 2015. Spatial heterogeneity of soil nutrients after the establishment of *Caragana intermedia* plantation on sand dunes in alpine sandy land of the Tibet Plateau. PLoS One 10, 1–12. https://doi.org/10.1371/journal.pone.0124456.

Li, B., Heijmans, M.M.P.D., Berendse, F., Blok, D., Maximov, T., Sass-Klaassen, U., 2016. The role of summer precipitation and summer temperature in establishment and growth of dwarf shrub *Betula nana* in northeast Siberian tundra. Polar Biol. 39, 1245–1255. https://doi.org/10.1007/s00300-015-1847-0.

Liu, J., 2011. The Study of Biologic Characteristics and Ecological Adaptability of *Caragana stenophylla*. Inner Mongolia University.

Ma, L., Zhou, Y., Chen, J., Cao, X., Chen, X., 2015. Estimation of fractional vegetation cover in semiarid areas by integrating endmember reflectance purification into nonlinear spectral mixture analysis. IEEE Geosci. Remote Sens. Lett. 12, 1175–1179. https://doi.org/10.1109/LGRS.2014.2385816.

Malkinson, D., Jeltsch, F., 2007. Intraspecific facilitation: a missing process along increasing stress gradients - insights from simulated shrub populations. Ecography 30, 339–348. https://doi.org/10.1111/j.2007.0906-7590.04983.x.

McGlynn, I.O., Okin, G.S., 2006. Characterization of shrub distribution using high spatial resolution remote sensing: ecosystem implications for a former Chihuahuan Desert grassland. Remote Sens. Environ. 101, 554–566. https://doi.org/10.1016/j.rse.2006.01.016.

Mishra, N.B., Crews, K.a., Neeti, N., Meyer, T., Young, K.R., 2015. MODIS derived vegetation greenness trends in African Savanna: deconstructing and localizing the role of changing moisture availability, fire regime and anthropogenic impact. Remote Sens. Environ. 169, 192–204. https://doi.org/10.1016/j.rse.2015.08.008.

Myers-Smith, I.H., Hallinger, M., Blok, D., Sass-Klaassen, U., Rayback, S.A., Weijers, S., Trant, A.J., Tape, K.D., Naito, A.T., Wipf, S., Rixen, C., Dawes, M.A., Wheeler, J.A., Buchwal, A., Baittinger, C., Macias-Fauria, M., Forbes, B.C., Levesque, E., Boulanger-Lapointe, N., Beil, I., Ravolainen, V., Wilmking, M., 2015. Methods for measuring arctic and alpine shrub growth: a review. Earth Sci. Rev. 140, 1–13. https://doi.org/10.1016/j.earscirev.2014.10.004.

Naito, A.T., Cairns, D.M., 2011. Patterns and processes of global shrub expansion. Prog. Phys. Geogr. 35, 423–442. https://doi.org/10.1177/0309133311403538.

Niu, X., 1999. The distribution and description of *Caragana* Fabr. in China. Acta Botan. Boreali-Occiden. Sin. 19, 107–133 (In Chinese).

Niu, Y., 2013. The characteristics of *Caragana intermedia* and its prospects for development. Inn. Mong. For. 3, 22–23 (in Chinese).

Peng, H.Y., Li, X.Y., Li, G.Y., Zhang, Z.H., Zhang, S.Y., Li, L., Zhao, G.Q., Jiang, Z.Y., Ma, Y.J., 2013. Shrub encroachment with increasing anthropogenic disturbance in the semiarid Inner Mongolian grasslands of China. Catena 109, 39–48. https://doi.org/10.1016/j.catena.2013.05.008.

Peng, H.Y., Li, X.Y., Tong, S.Y., 2014. Effects of shrub (*Caranaga Microphalla* Lam.) encroachment on water distribution and utilization in the typical steppe of Inner Mongolia. Acta Ecol. Sin. 34 (9), 2256–2265 (in Chinese).

Qiu, L., He, S., Jiang, D., Luo, Y., 2012. Regeneration patterns of *Caragana microphylla* in Horqin Sandy Land. Bull. Soil Water Conserv. 32, 176–179. https://doi.org/10.13961/j.cnki.stbctb.2012.04.066. (In Chinese).

Robinson, T.P., van Klinken, R.D., Metternicht, G., 2008. Spatial and temporal rates and patterns of mesquite (*Prosopis* species) invasion in Western Australia. J. Arid Environ. 72, 175–188. https://doi.org/10.1016/j.jaridenv.2007.05.011.

Sala, O.E., 2000. Global biodiversity scenarios for the year 2100. Science 287, 1770–1774. https://doi.org/10.1126/science.287.5459.1770.

Schlesinger, W.H., Abrahams, A.D., Parsons, A.J., Wainwright, J., 1999. Nutrient losses in runoff from grassland and shrubland habitats in Southern New Mexico: I. Rainfall simulation experiments. Biogeochemistry 45, 21–34. https://doi.org/10.1023/A:1006020831706.

Schweingruber, F., Poschlod, P., 2005. Growth rings in herbs and shrubs: life span, age determination and stem anatomy. For. Snow Landsc. Res. 79, 197–300.

Scurlock, J.M.O., Hall, D.O., 1998. The global carbon sink: a grassland perspective. Glob. Chang. Biol. 4, 229–233. https://doi.org/10.1046/j.1365-2486.1998.00151.x.

Seligman, N.G., Henkin, Z., 2000. Regeneration of a dominant Mediterranean dwarf-shrub after fire. J. Veg. Sci. 11, 893–902. https://doi.org/10.2307/3236559.

Selkowitz, D.J., 2010. A comparison of multi-spectral, multi-angular, and multi-temporal remote sensing datasets for fractional shrub canopy mapping in Arctic Alaska. Remote Sens. Environ. 114, 1338–1352. https://doi.org/10.1016/j.rse.2010.01.012.

Sohn, Y., Mccoy, R.M., 1997. Mapping desert shrub rangeland using spectral unmixing and modeling spectral mixtures with TM data. Photogramm. Eng. Remote. Sens. 63, 707–716.

Soliveres, S., Eldridge, D.J., 2014. Do changes in grazing pressure and the degree of shrub encroachment alter the effects of individual shrubs on understorey plant communities and soil function? Funct. Ecol. 28, 530–537. https://doi.org/10.1111/1365-2435.12196.

Swetnam, T.W., Allen, C.D., Betancourt, J.L., 1999. Applied historical ecology: using the past to manage for the future. Ecol. Appl. 9 (4), 1189–1206.

Tape, K.D., Hallinger, M., Welker, J.M., Ruess, R.W., 2012. Landscape heterogeneity of shrub expansion in Arctic Alaska. Ecosystems 15, 711–724. https://doi.org/10.1007/s10021-012-9540-4.

Tian, Y., Jia, Z., Yang, X., 2014. Improving shrub biomass estimations in the Qinghai-Tibet Plateau: age-based *Caragana intermedia* allometric models. For. Chron. 90, 154–160. https://doi.org/10.5558/tfc2014032.

Van Auken, O.W., 2009. Causes and consequences of woody plant encroachment into western North American grasslands. J. Environ. Manag. 90, 2931–2942. https://doi.org/10.1016/j.jenvman.2009.04.023.

Wang, J., Ni, J., 2009. Modelling the distribution of five *Caragana* species in temperate Northern China. Chin. J. Plant Ecol. 33, 12–24. https://doi.org/10.3773/j.issn.1005-264x.2009.01.002. (In Chinese).

Wang, W., Liang, C., Zhu, Z., Liu, Z., Zhang, L., 2001. Studies on the measuring method of growth rings of *Haloxylon ammodendron* and its growing dynamics. J. Arid Land Resour. Environ. 15, 67–74 (In Chinese).

Waser, L.T., Baltsavias, E., Ecker, K., Eisenbeiss, H., Feldmeyer-Christe, E., Ginzler, C., Küchler, M., Zhang, L., 2008. Assessing changes of forest area and shrub encroachment in a mire ecosystem using digital surface models and CIR aerial images. Remote Sens. Environ. 112, 1956–1968. https://doi.org/10.1016/j.rse.2007.09.015.

Wiegand, T., Milton, S.J., Esler, K.J., Midgley, G.F., 2000. Live fast, die young: estimating size-age relations and mortality pattern of shrubs species in the semi-arid Karoo, South Africa. Plant Ecol. 150, 115–131. https://doi.org/10.1023/A:1026526419886.

Wilfong, B.N., Gorchov, D.L., Henry, M.C., 2009. Detecting an invasive shrub in deciduous forest understories using remote sensing. Weed Sci. 57, 512–520. https://doi.org/10.1614/WS-09-012.1.

Wu, X., Ao, X., Yong, P., Zhang, C., Ru, H., 2016. Study on seed morphology and seedling growth characteristics of *Caragana* Genus Plants. Shanxi For. Sci. Technol. 45, 31–34 (In Chinese).

Xiong, X., Han, X., Bai, Y., Qingmin, P., 2003. Increased distribution of *Caragana microphylla* in rangelands and its causes and consequences in Xilin River Basin. Acta Prataculturae Sinica 12, 57–62 (In Chinese).

Zarovali, M.P., Yiakoulaki, M.D., Papanastasis, V.P., 2007. Effects of shrub encroachment on herbage production and nutritive value in semi-arid Mediterranean grasslands. Grass Forage Sci. 62, 355–363. https://doi.org/10.1111/j.1365-2494.2007.00590.x.

Zhao, X., Ren, J., 2005. Growth characteristics and its vegetation restoration significant of clonal of three *Caragana* species. Sci. Soil Water Conserv. 3, 102–107 (In Chinese).

Zhao, T., Zhao, N., Gao, Y., 2014. Effects of grazing exclusion on the composition and structure of steppe communities dominated by *Caragana microphylla*. Acta Ecol. Sin. 34, 4280–4287. https://doi.org/10.5846/stxb201212181816. (In Chinese).